ASME Journal of Turbomachinery
Online journal at:
https://asmedigitalcollection.asme.org/turbomachinery

Pawel J. Przytarski[1]
Department of Mechanical Engineering,
University of Melbourne,
Melbourne, Victoria 3010, Australia
e-mail: pawel.przytarski@unimelb.edu.au

Davide Lengani
DIME-University of Genova,
via alla Opera Pia 15,
Genova 16145, Italy
e-mail: davide.lengani@edu.unige.it

Daniele Simoni
DIME-University of Genova,
via alla Opera Pia 15,
Genova 16145, Italy
e-mail: daniele.simoni@unige.it

Andrew P. S. Wheeler
Whittle Laboratory,
Department of Engineering,
University of Cambridge,
Cambridge CB3 0DY, UK
e-mail: aw329@cam.ac.uk

The Role of Turbulence Transport in Mechanical Energy Budgets

In this article, we study the role of turbulence transport on loss prediction using high fidelity scale-resolving simulations. For this purpose, we use eight high-fidelity simulation datasets and compute flux of entropy and stagnation pressure transport equation budgets for all the cases. We find that under certain unsteady inflow conditions, the stagnation pressure coefficient is not a reliable loss metric even at low Mach number conditions. This is due to the turbulence transport terms. The impact of these terms, typically assumed to be negligible, made stagnation pressure loss coefficient underpredict loss from 0% to over 40% when compared to entropy loss coefficient for cases considered here. This effect was most pronounced for the cases with highly unsteady inflow conditions and at low Reynolds numbers.
[DOI: 10.1115/1.4065287]

Keywords: computational fluid dynamics (CFD), fluid dynamics and heat transfer phenomena in compressor and turbine components of gas turbine engines, energy dissipation, turbulence, unsteady flow

1 Introduction

High-fidelity simulations provide the details of the entire flow field in the blade passage and therefore may be used to explore loss generation and loss generating mechanisms [1]. The most commonly used loss metric is the stagnation pressure loss coefficient. This is because it can be directly measured and is a workhorse for evaluating the performance of different blade designs experimentally. There are other available metrics, such as entropy [2] or mechanical work potential [3], which have an advantage of better representing the lost work due to their ability to account for heat transfer and thermal mixing effects. However, they rely on quantities, which are difficult to measure or have to be derived (e.g., entropy cannot be measured directly). As a result, they are difficult to implement experimentally and lead to high levels of measurement uncertainty. It is therefore of interest to investigate complete transport equations using high-fidelity simulations and compare loss drivers between different loss metrics.

Transport equations have been practically used since the 1980*s*. Among the first, the work of Moore et al. [4] used mean part of the Reynolds decomposed transport equation of stagnation pressure (e.g., Ref. [5]) and applied it to the 2D-field measurements performed by means of hot-wire probes. They found that the integration of the production of the turbulence kinetic energy represented the generation of stagnation pressure loss well. Similarly, more recent articles, either experimental [6–8] or numerical [9,10], made strides to understand the mechanism by which turbulence extracts work from the mean flow via turbulence production. The interest in the production of turbulence kinetic energy is partially motivated by the relative ease of computing it from the experimental data with relatively low uncertainty. On the other hand, other terms appearing in the transport equations are difficult to obtain and are often neglected. For this reason, the transport equation of entropy that relates the entropy generation rate to the viscous dissipation and heat transfer terms has been computed in more recent high-fidelity simulations [11–16]. These authors showed that the full volume integration of the right- hand side of the entropy transport equation may provide a spatial breakdown of losses pointing out at their sources. In addition, Leggett et al. [15] provided a comparison of entropy and mechanical work potential terms appearing in the respective transport equations.

In the present article, we will compare different loss coefficients computed from several unsteady high-fidelity simulations of compressor blades, and we will further discuss the results computing the full transport equation of entropy and stagnation pressure flux. The article is structured as follow: (1) the global loss coefficients are introduced; (2) the numerical methods and simulation cases are summarized; (3) transport equations of entropy flux and stagnation pressure flux are analyzed to provide a rationale for a comparison of the metrics; and (4) the result section that discusses the different loss coefficients and loss budgets with a focus on the effect of turbulence on the different budgets. In particular, the article addresses the following questions:

(1) What determines the stagnation pressure and entropy loss coefficients?
(2) What drives the difference between the loss coefficients?
(3) When can we expect the two coefficients to vary?

[1]Corresponding author.

Contributed by the International Gas Turbine Institute (IGTI) of ASME for publication in the Journal of Turbomachinery. Manuscript received January 9, 2024; final manuscript received April 3, 2024; published online May 8, 2024. Tech. Editor: David G. Bogard.

Table 1 Details of two steady and six unsteady inflow cases

Geometry	Case	Re	Ma	F_{red}	Pu	Tu
NACA65	Tu4	140k	0.065	—	—	4.0%
NACA65	Tu6	140k	0.065	—	—	6.0%
NACA65	Gap30	140k	0.065	1.71	5.0%	4.2%
NACA65	Gap40	140k	0.065	1.71	3.6%	3.3%
NACA65	Gap50	140k	0.065	1.71	3.0%	2.9%
CDA	Gap30	250k	0.20	2.49	4.9%	3.1%
CDA	Gap40	250k	0.20	2.49	3.7%	2.9%
CDA	Gap50	250k	0.20	2.49	3.2%	3.0%

Table 2 Maximum near-wall viscous units

Case	*Mesh*	Δ_n^+	Δ_t^+	Δ_z^+
Steady *NACA65*	73M	0.9	7	7
Unsteady *NACA65*	130M	0.6	4.8	6.0
Unsteady *CDA*	170M	0.9	15.5	10.0

Finally, the article demonstrates why entropy loss coefficient does not match stagnation pressure loss coefficient despite adiabatic and subsonic flow conditions.

2 Computational Setup

2.1 Solver Details. For this study, we use high-fidelity datasets of Przytarski and Wheeler [12,14]. These datasets were generated using the high-order compressible Navier–Stokes solver 3*DNS* [17]. In total, eight datasets were used which consisted of two *NACA*65 datasets at steady turbulent inflow conditions, three *NACA*65 datasets at unsteady inflow conditions akin to multistage environment, and three *CDA* (Controlled Diffusion Airfoil) datasets unsteady inflow conditions akin to multistage environment. Table 1 summarizes the datasets and shows the running conditions of each case. For cases with unsteady inflow conditions reduced frequency F_{red} was also reported, and the unsteadiness intensity was decomposed into periodic Pu and turbulent Tu components. The spanwise extent for *NACA*65 cases was 10% of the axial chord, while *CDA* cases used spanwise extent equal to 15% of axial chord. Maximum viscous wall for these geometries are reported in Table 2 asserting the wall-resolved accuracy. Setup details and a more thorough description of each case, including a procedure used to mimic the multistage environment, can be found in Refs. [12,14]. An example of an instantaneous flowfield for steady and unsteady *NACA*65 profile as well as an unsteady *CDA* profile is shown in Fig. 1 for which the spanwise vorticity contours were plotted.

3 Loss Metrics

As discussed by Denton [2], there are several loss coefficients that are used in turbomachinery. The most popular loss coefficients are entropy, enthalpy, and stagnation pressure loss coefficients. As asserted by Denton [2], entropy and enthalpy loss coefficients should report virtually identical results. However, the advantage of entropy loss coefficient is that it is more applicable in the engine setting. More in-depth discussion on the limitations of each loss coefficient can be found in the literature [18,19]. Despite the consensus that entropy loss coefficient is the most accurate for engine performance evaluation, the industrial practice often relies on stagnation pressure loss coefficient due to the ease of measuring it in an experimental setting. However, in our experience, it is often difficult to obtain consistent results from entropy and stagnation pressure loss coefficients. Given the availability of relevant high-fidelity datasets, it is desirable to study the predictive capability of these loss coefficients, what determines them and their limitations for the unsteady, turbulent turbomachinery flows.

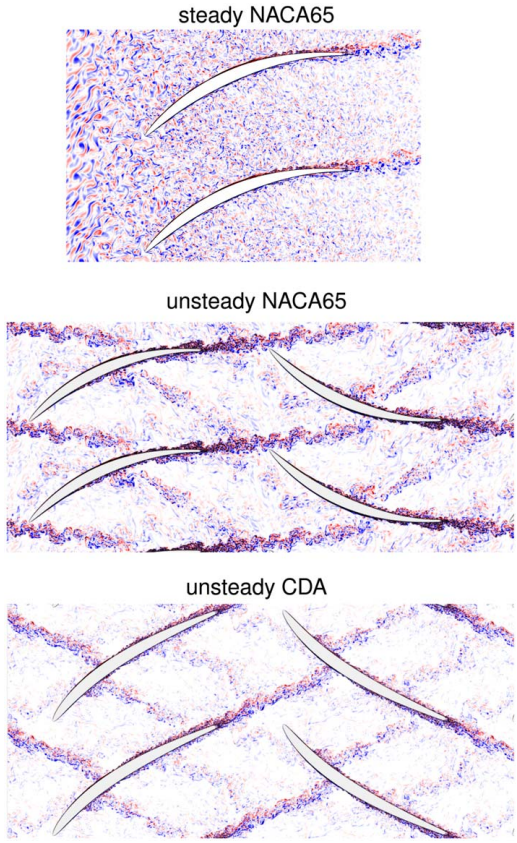

Fig. 1 Instantaneous spanwise vorticity flowfield for three example cases considered here: *NACA65 – Tu4* (top), *NACA65 – Gap40* (center), and *CDA – Gap40* (bottom)

3.1 Entropy Loss Coefficient. Entropy loss coefficient can be computed from high-fidelity data directly by taking time-averaged and flux-averaged entropy at the inlet and outlet of the integration domain:

$$\omega^s = \frac{T_2(s_2 - s_1)}{h_{t,1} - h_1} \tag{1}$$

Alternatively, entropy can be approximated with time-averaged and mass-averaged pressure and temperature:

$$s - s_{\text{ref}} = C_p \ln\left(\frac{T}{T_{\text{ref}}}\right) - R \ln\left(\frac{p}{p_{\text{ref}}}\right) \tag{2}$$

to compute the derived entropy loss coefficient:

$$\omega^{s_{(T,p)}} = \frac{T_2(s_{(T,p)2} - s_{(T,p)1})}{h_{t,1} - h_1} \tag{3}$$

3.2 Enthalpy Loss Coefficient. Enthalpy loss coefficient (time averaged and mass averaged) can be computed according to:

$$\omega^h = \frac{h_2 - h_{2s}}{h_{t,1} - h_1} \tag{4}$$

and is a popular choice for the design practice as it is independent of the Mach number.

3.3 Stagnation Pressure Loss Coefficient. The stagnation pressure loss coefficient can be obtained experimentally by directly measuring total pressure, which can be time averaged and mass averaged:

$$\omega^p = \frac{p_{t,1} - p_{t,2}}{p_{t,1} - p_1} \tag{5}$$

Table 3 The summary of loss coefficients for all the cases

	NACA65		*NACA65*			*CDA*		
Loss	Tu4	Tu6	Gap30	Gap40	Gap50	Gap30	Gap40	Gap50
ω^s	0.0290	0.0383	0.0271	0.0259	0.0262	0.0229	0.0208	0.0208
$\omega^{s(T,p)}$	0.0296	0.0390	0.0284	0.0267	0.0270	0.0234	0.0213	0.0212
ω^h	0.0296	0.0390	0.0284	0.0267	0.0270	0.0235	0.0213	0.0212
ω^p	**0.0255**	**0.0287**	**0.0145**	**0.0186**	**0.0205**	**0.0207**	**0.0207**	**0.0206**
$\omega^p_{no\,TKE}$	**0.0225**	**0.0180**	**0.0067**	**0.0128**	**0.0161**	**0.0149**	**0.0151**	**0.0153**

Note: Bold values correspond to typically computed mass-averaged stagnation pressure loss coefficients which for the cases considered here underestimate the loss when compared with similarly computed entropy and enthalpy loss coefficients.

This is the most commonly used loss coefficient, and it is generally accepted that it is an accurate estimate, at least in the limit of low Mach numbers. When stagnation pressure is measured at sufficiently high frequency at incompressible limit, the stagnation pressure formula reads:

$$p_t = \bar{p} + \frac{1}{2}\bar{u}_i\bar{u}_i + \frac{1}{2}\overline{u_i'u_i'} \tag{6}$$

where $(1/2)\bar{u}_i\bar{u}_i$ represents mean kinetic energy and $(1/2)\overline{u_i'u_i'}$ represents turbulent kinetic energy. However, in practice, when unsteadiness is low enough, turbulent part of the kinetic energy is discarded resulting in:

$$p_{t,no\,TKE} = \bar{p} + \frac{1}{2}\bar{u}_i\bar{u}_i \tag{7}$$

Equations (6) and (7) are in practice used interchangeably, but at highly unsteady flowfields, they result in different stagnation pressure estimates and may have an impact in particular when comparing experimental results against Reynolds-averaged Navier–Stokes (RANS)-derived predictions. Definition in Eq. (6) arises from the total kinetic energy transport equation that will be shown later (Eq. (15)), while definition in Eq. (7) arises from the mean part of the kinetic energy transport equation, shown in Appendix A (Eq. (20a)). Both of these definitions can be used to obtain a mass-averaged stagnation pressure loss coefficient, which will be referred to as follows:

ω^p—for stagnation pressure including TKE
$\omega^p_{no\,TKE}$—for stagnation pressure without TKE

In this paper, we will explore the impact of turbulent kinetic energy on these predictions and the role turbulent transport plays in stagnation pressure loss coefficient in general.

4 Evaluation of Loss Coefficients

Table 3 gives a summary of above mentioned loss coefficients for all the cases considered here. For the steady cases, i.e., *NACA*65 *Tu*4 and *Tu*6, the reference planes that were used to compute the loss coefficients were set at 30% axial chord upstream of the leading edge and downstream of the trailing edge. For the unsteady cases, the reference planes were set at the domain inlet (20–40% upstream of the leading edge depending on the gap) and at the sampling plane, which was located at roughly 10% axial chord downstream of the trailing edge. As evident from the Table 3, both entropy and enthalpy loss coefficients result in closely matching estimates. On the other hand, the mass-averaged pressure loss coefficient (ω^p) results in values which are not only quantitatively different but also qualitatively misleading by reversing the loss trend for unsteady *NACA*65 cases. These values were highlighted in bold. The estimates are even worse when mass-averaged stagnation pressure loss coefficient without the inclusion of turbulent kinetic energy ($\omega^p_{no\,TKE}$) is considered (also highlighted in bold). This emphasizes the need of including turbulent kinetic energy for mass-averaged stagnation pressure estimates when highly unsteady flowfields are considered. To understand why the mass-averaged stagnation pressure coefficient (ω^p) is inaccurate, in the next section, we will examine entropy and stagnation pressure transport equations.

5 Loss Transport Equations

The loss coefficients give us an estimate of losses in a global sense so that an overall performance of a system can be assessed. However, with all the information that high-fidelity datasets offer, these losses can be studied in more detail by examining their transport equations. Here, specifically, we will consider entropy transport equation and kinetic energy transport equation. To study these transport equations, all the quantities will be integrated in the volume, Ω, between the same reference planes as were used for the computations of loss coefficients. Throughout the article, the integrated quantities are capitalized, for instance, the integrated dissipation will be:

$$\Phi = \int_\Omega \phi d\Omega \tag{8}$$

and since the simulation were compressible, all quantities used in the budgets are Favre-averaged:

$$\tilde{f} \equiv \frac{\overline{\rho f}}{\bar{\rho}} \tag{9}$$

5.1 Entropy Transport Equation. First, we examine the entropy transport equation [20]:

$$\rho\frac{\mathrm{D}s}{\mathrm{D}t} = \left(\frac{1}{T}\tau_{ij}\frac{\partial u_i}{\partial x_j}\right) + \kappa\left(\frac{(\nabla T)^2}{T^2}\right) - \left(\nabla\cdot\frac{q}{T}\right) \tag{10}$$

To gain further insight, we may decompose the flowfield into mean and turbulent components by performing Reynolds decomposition:

$$f = \bar{f} + f' \tag{11}$$

For the purpose of comparing entropy with stagnation pressure loss metrics, we rearrange the equation so that the left-hand side is akin to $T\Delta s$ term, while the right-hand side has contributions, which are due to the viscous dissipation and heat transfer terms. Following a similar procedure as the one outlined in Ref. [21], we obtain:

$$\underbrace{\overline{T\rho\frac{Ds}{Dt}}}_{ts} = \underbrace{\bar{\tau}_{ij}\frac{\partial\bar{u}_i}{\partial x_j}}_{\phi_m} + \underbrace{\overline{\tau'_{ij}\frac{\partial u'_i}{\partial x_j}}}_{\phi_f} + \underbrace{\kappa\frac{1}{\bar{T}}\left(\frac{\partial\bar{T}}{\partial x_i}\right)^2}_{irq_m} - \underbrace{\bar{T}\frac{\partial}{\partial x_i}\left(\frac{\bar{q}_i}{\bar{T}}\right)}_{rq_m} - \underbrace{\bar{T}\frac{\partial}{\partial x_i}\left(\frac{\bar{q}'_i}{\bar{T}}\right)}_{rq_f} \tag{12}$$

where ts is the entropy generation rate, ϕ_m is the viscous dissipation due to mean strains, ϕ_f is the turbulent viscous dissipation, irq_m is the mean flow irreversible heat transport, rq_m is the mean flow reversible heat flux, and rq_f is the turbulent reversible heat flux

The first two terms on the right-hand side are the irreversible entropy changes due to viscous friction, while the terms three,

four, and five are the irreversible and reversible changes in entropy due to heat transfer. For the cases considered in this article, integrated heat transfer terms are negligible (adiabatic, low Mach numbers). It is also important to point out that in a computational sense, another term comes about, ε_N, due to the combined effects of discretization errors and numerical filtering (artificial dissipation). As a result for cases considered here, the flux of entropy budgets can be computed as follows:

$$\underbrace{\int \overline{T\rho \frac{\mathrm{D}s}{\mathrm{D}t}}\,\mathrm{d}\Omega}_{TS_T} \approx \underbrace{\int \left(\overline{\bar{\tau}_{ij}\frac{\partial \bar{u}_i}{\partial x_j}}\right)\mathrm{d}\Omega}_{\Phi_m} + \underbrace{\int \left(\overline{\tau'_{ij}\frac{\partial u'_i}{\partial x_j}} + \varepsilon_N\right)\mathrm{d}\Omega}_{\Phi_{f+N}} \tag{13}$$

Equation (13) suggests that for adiabatic flows at low Mach numbers, entropy comes about purely as a result of viscous dissipation. It also allows for the estimation of artificial dissipation term, ε_N, caused by the insufficient mesh resolution. This fact was previously used by Przytarski and Wheeler [14] to assess the simulation resolution and a more in-depth discussion of entropy budgets can be found there. We further assert that the artificial dissipation can be accounted to the turbulent viscous dissipation by performing Reynolds decomposition of kinetic energy transport equation and computing full budget for both mean and turbulent components. This is shown in Appendix A. Consequently, for the remainder of the article, we will refer to the combined resolved and unresolved turbulent viscous dissipation as Φ_{f+N}.

5.2 Stagnation Pressure Transport Equation. To obtain the stagnation pressure transport equation (same as kinetic energy transport equation), momentum and continuity equations can be rearranged to obtain:

$$\frac{\mathrm{D}p_t}{\mathrm{D}t} \approx \frac{D\left(\rho(1/2)u_iu_i\right)}{\mathrm{D}t} + u_i\frac{\partial p}{\partial x_j} = u_i\frac{\partial \tau_{ij}}{\partial x_j} \tag{14}$$

As mentioned earlier, we can gain more insight by decomposing the flowfield into mean and turbulent components by performing Reynolds decomposition and averaging with respect to time as shown in Ref. ([22], p. 71):

$$\begin{aligned}
&\underbrace{\bar{u}_i\frac{\partial \bar{p}_t}{\partial x_i}}_{fsp} \approx \underbrace{\bar{u}_i\frac{\partial}{\partial x_j}\left(\bar{\rho}\frac{1}{2}\bar{u}_i\bar{u}_i\right)}_{adv_m} + \underbrace{\bar{u}_i\frac{\partial}{\partial x_j}\left(\bar{\rho}\frac{1}{2}\overline{u'_iu'_i}\right)}_{adv_f} + \underbrace{\bar{u}_i\frac{\partial \bar{p}}{\partial x_i}}_{pw_m} = \\
&\quad \underbrace{-\bar{\tau}_{ij}\frac{\partial \bar{u}_i}{\partial x_j}}_{\phi_m} \underbrace{-\overline{\tau'_{ij}\frac{\partial u'_i}{\partial x_j}}}_{\phi_f} \underbrace{-\frac{\partial}{\partial x_j}\left[\bar{u}_i\left(\overline{\rho u'_iu'_j}\right)\right]}_{tr_{mf}} \underbrace{-\frac{\partial}{\partial x_j}\left[\overline{\rho u'_j\left(\frac{1}{2}u'_iu'_i\right)}\right]}_{tr_{ff}} \\
&\quad \underbrace{+\frac{\partial \bar{\tau}_{ij}\bar{u}_i}{\partial x_j}}_{vd_m} \underbrace{+\frac{\partial \overline{\tau'_{ij}u'_i}}{\partial x_j}}_{vd_f} \underbrace{+\bar{u}'_i\frac{\partial \bar{p}}{\partial x_i}}_{pw_f} \underbrace{-\frac{\partial \overline{p'u'_i}}{\partial x_i}}_{pd_f} \underbrace{+\overline{p'\frac{\partial u'_i}{\partial x_i}}}_{pl_f}
\end{aligned} \tag{15}$$

where *fsp* is the mean flow of stagnation pressure, *adv* is the convection of kinetic energy, *pw* is the pressure work, *tr* is the turbulent transport due to unsteadiness, *vd* is the viscous diffusion, ϕ is the viscous dissipation, *pd* is the pressure diffusion, and *pl* is the pressure dilation.

6 Loss Transport Equations Budgets and Loss Coefficients

Entropy and stagnation pressure transport equations can be directly related to loss coefficients:

$$\omega^s(\mathrm{TS}_T) = \frac{T_2(s_2 - s_1)}{h_{t,1} - h_1} \approx \frac{1}{h_{t,1} - h_1}\frac{\mathrm{TS}_T}{\dot{m}} \tag{16a}$$

$$\omega^p(\mathrm{FSP}) = \frac{p_{t,1} - p_{t,2}}{p_{t,1} - p_1} \approx \frac{\rho_{\mathrm{ref}}}{p_{t,1} - p_1}\frac{-\mathrm{FSP}}{\dot{m}} \tag{16b}$$

as a result, we are now able to split each loss coefficient into its constituent components and comment directly on their relative importance:

$$\mathrm{TS}_T = \Phi_m + (\Phi_{f+N}) \tag{17a}$$

$$\begin{aligned}
-FSP = \Phi_m + (\Phi_{f+N}) \\
+ \underbrace{\mathrm{Tr}_{mf} + \mathrm{Tr}_{ff} - \mathrm{VD}_m - \mathrm{VD}_f - \mathrm{PW}_f + \mathrm{PD}_f - \mathrm{PL}_f}_{\text{typically assumed}\approx 0}
\end{aligned} \tag{17b}$$

As mentioned earlier, for cases considered here, the entropy loss coefficient is driven purely by the viscous dissipation, conveniently split into dissipation due to mean strains Φ_m and turbulent dissipation Φ_{f+N} (the sum of resolved and unresolved components).

The stagnation pressure loss coefficient arise as an interplay between dissipation due to mean strains Φ_m, turbulent dissipation Φ_{f+N}, turbulent transport due to mean and turbulent fields Tr_{mf} and Tr_{ff}, mean and turbulent viscous diffusion VD_m and VD_f, as well as turbulent pressure work PW_f, pressure diffusion PD_f, and pressure dilation PL_f. It should be mentioned that since Moore et al. [4], the diffusive terms ($\mathrm{Tr}_{mf,ff}$, $\mathrm{VD}_{m,f}$, PW_f, PD_f, PL_f) are often neglected as it is assumed that their volume integral is negligible. Furthermore, there are practical difficulties estimating these terms experimentally. High-fidelity datasets are immune to such limitations and so are perfect test bed for verifying these assumptions under a variety of conditions. Table 4 shows the entropy transport equation budgets for all the cases. Below the budget, entropy loss coefficient derived from the budget is compared to the one computed globally at the reference frames. Very good agreement is shown between these two loss coefficients.

Table 4 Entropy transport equation budgets

$\mathrm{TS}_T \approx \Phi_m + \Phi_{f+N}$								
	NACA65		NACA65			CDA		
	Tu4	Tu6	Gap30	Gap40	Gap50	Gap30	Gap40	Gap50
TS_T	7.564	9.954	6.980	6.668	6.726	2111.269	1916.130	1916.756
Φ_m	3.588	3.660	3.419	3.472	3.554	962.015	904.669	911.772
Φ_{f+N}	3.976	6.295	3.561	3.196	3.172	1149.254	1011.461	1004.984
$\omega^s(\mathrm{TS}_T)$	0.0295	0.0388	0.0272	0.0260	0.0263	0.0234	0.0213	0.0213
ω^s_m	0.0290	0.0383	0.0271	0.0259	0.0262	0.0229	0.0208	0.0208

Table 5 Flux of stagnation pressure transport equation budgets

$$-\text{FSP} = \Phi_m + \Phi_{f+N} + \text{Tr}_{mf} + \text{Tr}_{ff} - \text{VD}_m - \text{VD}_f - \text{PW}_f + \text{PD}_f - \text{PL}_f$$

	NACA65		NACA65			CDA		
	Tu4	Tu6	Gap30	Gap40	Gap50	Gap30	Gap40	Gap50
$-\text{FSP} = -\text{Adv}_m - \text{Adv}_f - \text{PW}_m$	6.691	7.576	3.811	4.801	5.308	1,816.369	1,891.532	1,929.971
Φ_m	3.588	3.660	3.419	3.472	3.554	962.015	904.669	911.772
Φ_{f+N}	3.976	6.295	3.561	3.196	3.172	1149.254	1011.461	1004.984
Tr_{mf}	−0.847	−2.587	−3.905	−2.551	−2.004	−387.640	−207.121	−208.588
Tr_{ff}	—	—	0.688	0.649	0.488	94.282	213.863	202.576
$-\text{VD}_m$	−0.012	−0.009	−0.014	−0.015	−0.015	−2.451	−2.229	−2.240
$-\text{VD}_f$	−0.008	−0.017	−0.005	−0.005	−0.005	−1.881	−1.577	−1.544
$-\text{PW}_f$	—	—	—	—	—	—	—	—
PD_f	—	-	0.129	0.080	0.111	4.810	26.336	33.456
$-\text{PL}_f$	—	—	—	—	—	—	—	—
LHS–RHS	−0.073	−0.315	0.054	0.016	−0.016	−41.965	13.668	−32.144
ω^p(FSP)	0.0264	0.0298	0.0149	0.0187	0.0208	0.0204	0.0212	0.0217
ω^p_m	0.0255	0.0287	0.0145	0.0186	0.0205	0.0207	0.0207	0.0206

Similarly, Table 5 shows the stagnation pressure transport equation budgets for all the cases. At the bottom of the table, the stagnation pressure loss coefficient derived from the budget is compared to the one computed globally and, again, a good agreement is shown between these two loss coefficients for all the cases.

Some of the terms in the stagnation pressure transport equation budgets (mainly PW_f, PL_f) were not possible to compute and as a result were not considered. Despite omitting them in the budget, the difference between left-hand side and the right-hand side terms (LHS-RHS) is small, and it is therefore concluded that these terms can be considered negligible for the cases considered here.

In the next section, we will explore how the components of these loss budgets determine the overall loss coefficient.

7 Comparison of Loss Contributions

The first thing to note from Table 5 is that while most diffusive terms are indeed close to zero and negligible as typically assumed; however, the turbulent transport terms Tr_{mf} and Tr_{ff} are consistently high and range from 15% of turbulence dissipation Φ_f for the moderate turbulence *NACA*65 *Tu*4 case, all the way to over 100% for the unsteady *NACA*65 *Gap*30 case.

This is further demonstrated by integrating all the budgets along the streamwise direction to obtain a line integral plots for the steady *NACA*65 *Tu*4 case, Fig. 2, unsteady *NACA*65 *Gap*40 case, Fig. 3, and unsteady *CDA Gap*40 case, Fig. 4. For all the cases, the domain was normalized by the axial chord with $x = 0$ coordinate corresponding to the leading edge and $x = 1$ coordinate corresponding to the trailing edge.

Turbulent transport terms Tr_{mf} and Tr_{ff} play a significant role in stagnation pressure transport equation for most of the considered cases. For *CDA* cases, their impact appears to be limited as both terms are of similar magnitude and opposite sign and therefore lead to error cancellation.

It can be also noted that turbulent transport terms have a stronger impact on the cases that feature more unsteady/turbulent inflow. As a result, by the virtue of how stagnation pressure transport is computed and due to the terms' negative contribution, they reduce the stagnation pressure loss coefficient, resulting in erroneous performance prediction.

To understand where the impact of turbulent transport terms is the strongest, we perform a domain decomposition and compute a loss budget for different regions. We determine the boundary layer and the wake edges with a vorticity criterion. Figure 5 shows the resulting region split. Figure 6 shows separate budgets for the combined regions of boundary layers and wake and for the freestream for the steady inflow *NACA*65 *Tu*4 case. Similarly, Fig. 7 shows analogous budget for the unsteady inflow *NACA*65 *Gap*40 case and Fig. 8 shows that for the unsteady inflow *CDA*

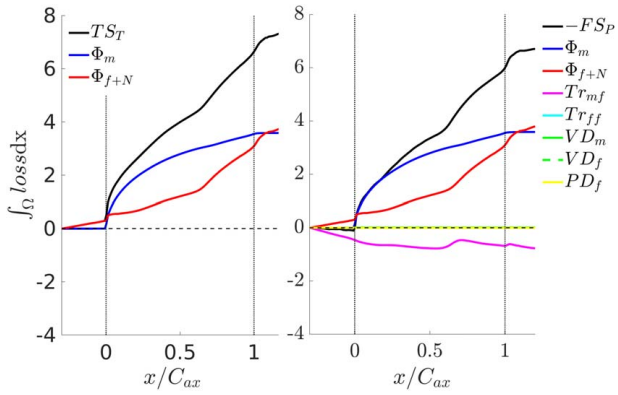

Fig. 2 Comparison of loss contributions to entropy (left) and stagnation pressure (right) loss metrics for the steady inflow *NACA65 Tu4* case

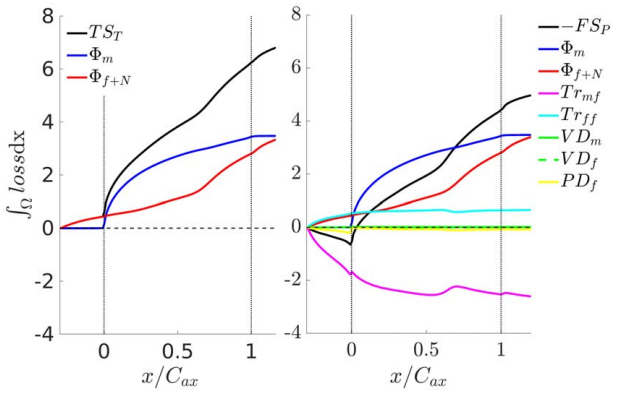

Fig. 3 Comparison of loss contributions to entropy (left) and stagnation pressure (right) loss metrics for the unsteady inflow *NACA65 Gap40* case

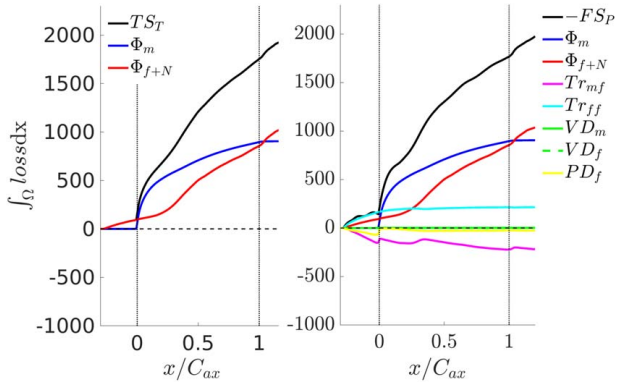

Fig. 4 Comparison of loss contributions to entropy (left) and stagnation pressure (right) loss metrics for the unsteady inflow *CDA65 Gap40* case

Fig. 5 Example domain decomposition for the *NACA65 Tu4* case

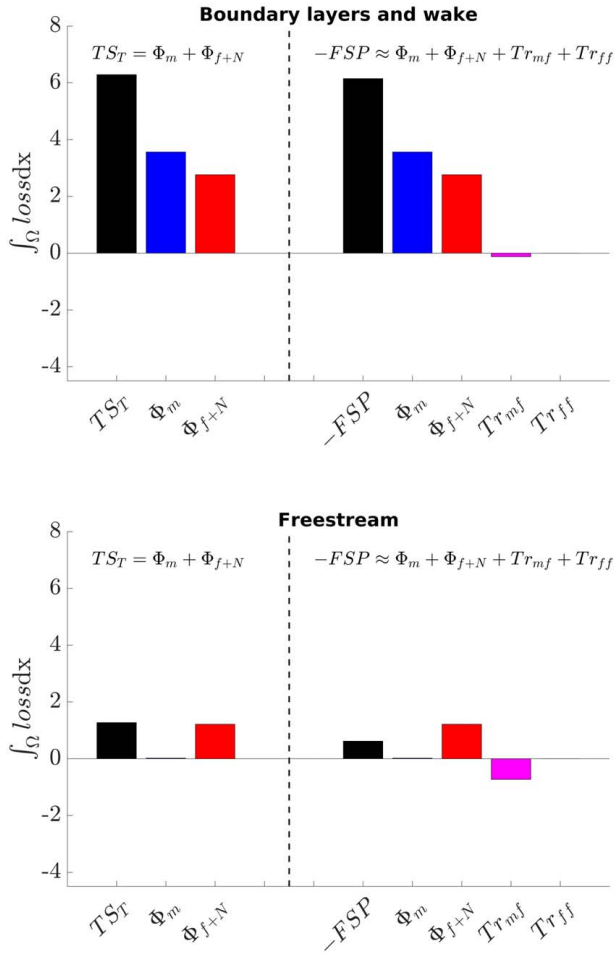

Fig. 6 Comparison of loss contributions for the steady inflow *NACA65 Tu4* case for boundary layers and wake (top) and freestream (bottom)

*Gap*40 case. The overall loss comparison for the remaining cases is given in Table 6. It is clear from both figures that majority of turbulent transport Tr_{mf} and Tr_{ff} happens in the freestream. As a result, the loss, as predicted by stagnation pressure, is well predicted for the boundary layers and wake regions; however, it reduces in the freestream, which skews the overall loss prediction. This was the case for most of the datasets considered here. For two *CDA* cases with *Gap*40 and *Gap*50, that effect was negligible as the two turbulent transport terms were of similar magnitude and opposite signs.

The results suggest that even for the cascades exposed to moderate levels of freestream turbulence, stagnation pressure loss coefficient may lead to incorrect predictions, especially when cases with varying or unsteady inflow conditions are considered.

To understand why turbulent transport by the mean flow Tr_{mf} is negative, we can inspect the formula behind the term:

$$\mathrm{tr}_{mf} = \frac{\partial}{\partial x_j}\left[\bar{u}_i\left(\overline{\rho u_i' u_j'}\right)\right] \tag{18}$$

In the freestream, the Reynolds stress terms $(\overline{\rho u_i' u_j'})$ are expected to universally decay at the steady rate. For a compressor, this decay is combined with a flow deceleration $(\bar{u}_i)$. As a result (also because of the sign of the term), the overall contribution to the stagnation pressure budget is negative, artificially lowering the predicted loss. We expect this to be the case when meaningful levels of turbulence/periodic unsteadiness(2–3% or above) is present. The erroneous stagnation pressure loss coefficient behavior happens irrespective of low Mach number conditions and is purely related to the freestream unsteadiness and turbulence transport term that arise due to it.

To understand why turbulent transport by the turbulent flow Tr_{ff} is positive for the unsteady inflow cases considered here, we can inspect the formula behind the term:

$$\mathrm{tr}_{ff} = \frac{\partial}{\partial x_j}\left[\overline{\rho u_j'\left(\frac{1}{2}u_i' u_i'\right)}\right] \tag{19}$$

The unsteady inflow cases consisted of periodic wakes, which have an appearance of u' and v' fluctuations. These fluctuations grow in size as the wake is initially accelerated and turned when entering the passage and subsequently diffused in the aft portion of it. Such behavior would result first in an increase of Tr_{ff} term and then its slow reduction. Figures 3 and 4 suggest that the initial acceleration and turning dominate and determine the magnitude of this term, which then stays relatively constant for the remainder of the passage where it is diffused.

We can also determine which components of the turbulent transport contribute the most. This is shown in Table 7, which demonstrates that for the cases considered here two terms associated with the $u'u'$ and $u'v'$ Reynolds stresses are responsible for the entire turbulent transport Tr_{mf} (other terms were close to 0). This is encouraging as it suggests that at a mid-span section the turbulent transport term can be successfully estimated experimentally by considering only these two components alone and measuring Reynolds stress components associated with them. This has been demonstrated before by Perdichizzi et al. [23] or Jelly et al. [24]. The role of the turbulent transport term Tr_{mf} was also previously recognized by Folk et al. [25,26] who used rapid distortion theory to estimate the magnitude of this term

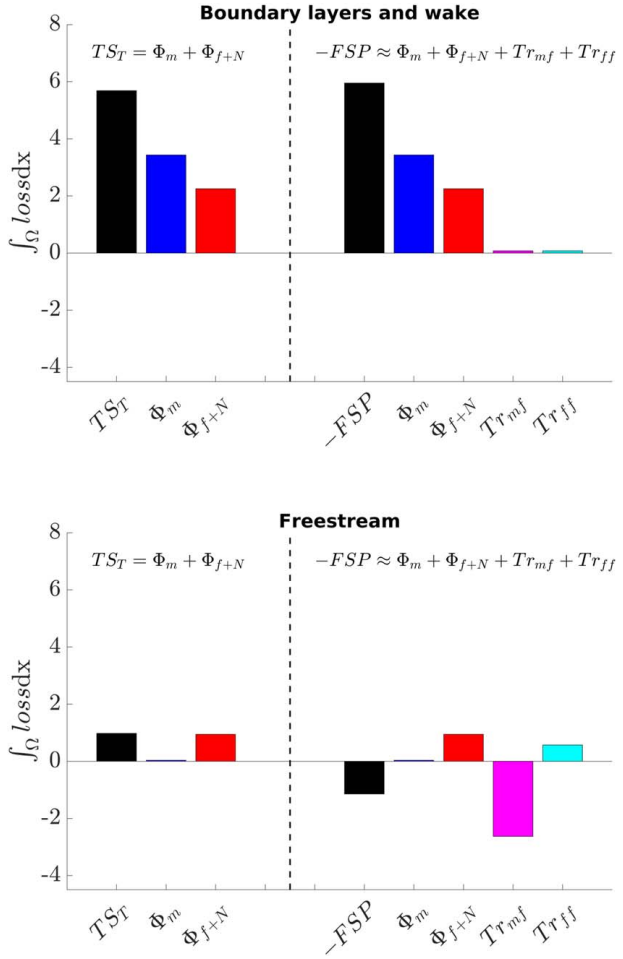

Fig. 7 Comparison of loss contributions for the unsteady inflow *NACA65 Gap40* case for boundary layers and wake (top) and freestream (bottom)

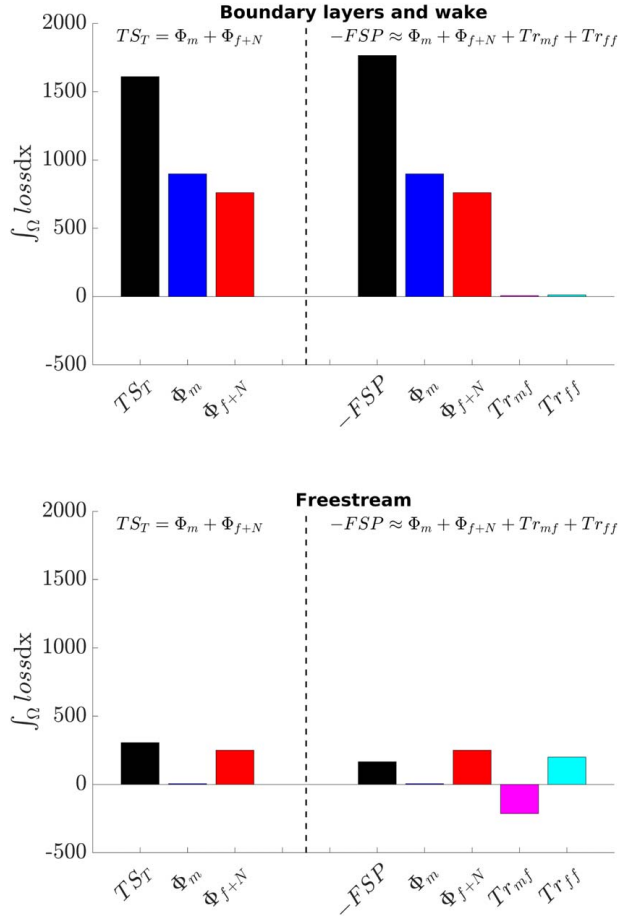

Fig. 8 Comparison of loss contributions for the unsteady inflow *CDA Gap40* case for boundary layers and wake (top) and freestream (bottom)

for turbine flow exposed to combustor turbulence. As far as Tr_{ff} term is concerned, it appears to be entirely determined by the streamwise fluctuations u' and turbulent kinetic energy $(1/2)u_i'u_i'$.

8 Gibbs Equation

The Gibbs equation accounts for the changes in fluid properties along the flow path and relates the change in enthalpy to the change in entropy and pressure. This relationship can be applied to stagnation properties of the flow as follows:

$$T_t \frac{\mathrm{D}s}{\mathrm{D}t} = \frac{\mathrm{D}h_t}{\mathrm{D}t} - \frac{1}{\rho_t}\frac{\mathrm{D}p_t}{\mathrm{D}t} \tag{20}$$

When considering adiabatic flow through a stationary blade row, stagnation temperature is constant, consequently:

$$T_t \frac{\mathrm{D}s}{\mathrm{D}t} \approx -\frac{1}{\rho_t}\frac{\mathrm{D}p_t}{\mathrm{D}t} \tag{21}$$

Table 6 Entropy and stagnation pressure loss prediction for the combined region of boundary layers and wake and for freestream

	NACA65		*NACA65*			*CDA*		
	Tu4	Tu6	Gap30	Gap40	Gap50	Gap30	Gap40	Gap50
$TS_{T,\mathrm{tot}}$	7.564	9.954	6.980	6.668	6.726	2111.269	1916.130	1916.756
$-FSP_{\mathrm{tot}}$	6.770	7.656	3.819	4.810	5.317	1860.353	1931.734	1972.560
$TS_{T,\mathrm{blw}}$	6.289	6.616	5.836	5.688	5.789	1771.757	1610.546	1627.988
$-FSP_{\mathrm{blw}}$	6.149	6.331	6.338	5.953	5.956	1449.368	1441.570	1424.509
$TS_{T,\mathrm{free}}$	1.2752	3.3381	1.1441	0.9799	0.9377	339.5117	305.5845	288.7683
$-FSP_{\mathrm{free}}$	0.622	1.325	−2.519	−1.143	−0.639	410.985	490.164	548.050
$-FSP_{\mathrm{blw}}/TS_{T,\mathrm{blw}}$	97.77%	95.69%	108.61%	104.66%	102.90%	96.43%	106.38%	102.90%
$-FSP_{\mathrm{free}}/TS_{T,\mathrm{free}}$	48.76%	39.70%	−220.16%	−116.63%	−68.17%	36.17%	64.81%	102.99%

Table 7 Contribution of different components to turbulent transport Tr_{mf}

	NACA65		NACA65			CDA		
	Tu4	Tu6	Gap30	Gap40	Gap50	Gap30	Gap40	Gap50
$\frac{\partial}{\partial x}\left[\bar{u}\left(\overline{\rho u' u'}\right)\right]/\mathrm{Tr}_{mf}$	0.74	0.85	1.09	1.14	1.13	2.45	3.82	3.64
$\frac{\partial}{\partial x}\left[\bar{v}\left(\overline{\rho u' v'}\right)\right]/\mathrm{Tr}_{mf}$	0.26	0.15	−0.09	−0.14	−0.14	−1.44	−2.79	−2.61
$\frac{\partial}{\partial x}\left[\overline{\rho u'\left(\frac{1}{2}u'u'\right)}\right]/\mathrm{Tr}_{ff}$	—	—	0.87	0.87	0.86	0.67	0.74	0.74
$\frac{\partial}{\partial x}\left[\overline{\rho u'\left(\frac{1}{2}v'v'\right)}\right]/\mathrm{Tr}_{ff}$	—	—	0.07	0.07	0.07	0.25	0.22	0.21
$\frac{\partial}{\partial x}\left[\overline{\rho u'\left(\frac{1}{2}w'w'\right)}\right]/\mathrm{Tr}_{ff}$	—	—	0.06	0.06	0.07	0.08	0.05	0.04

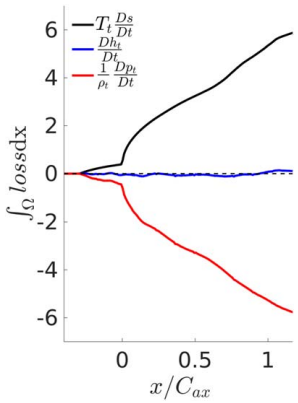

Fig. 9 Gibbs equation budget for the unsteady inflow *CDA65 Gap40* case

This is demonstrated to be true in Fig. 9 for which a series of 500 instantaneous snapshots were used to compute Gibbs equation budgets in their compressible form. This assertion often leads to a conclusion that

$$\Delta s \approx -R \ln\left(\frac{p_{t,2}}{p_{t,1}}\right) \tag{22}$$

However, as shown earlier, this does not hold for the data presented. To explain why that is we perform Reynolds decomposition on incompressible stagnation pressure:

$$\frac{\mathrm{D}p_t}{\mathrm{D}t} \approx \frac{\mathrm{D}}{\mathrm{D}t}\left(p + \frac{1}{2}\rho u_i u_i\right) \tag{23}$$

and find:

$$\begin{aligned}\frac{\overline{Dp_t}}{Dt} \approx & \underbrace{\frac{\bar{D}}{Dt}\left(\bar{\rho}\frac{1}{2}\bar{u}_i\bar{u}_i\right)}_{adv_m} + \underbrace{\frac{\bar{D}}{Dt}\left(\bar{\rho}\frac{1}{2}\overline{u_i'u_i'}\right)}_{adv_f} + \underbrace{\bar{u}_i\frac{\partial\bar{p}}{\partial x_i}}_{pw_m} \\ & \underbrace{-\frac{\partial}{\partial x_j}\left[\bar{u}_i\left(\overline{\rho u_i'u_j'}\right)\right]}_{tr_{mf}} \underbrace{-\frac{\partial}{\partial x_j}\left[\overline{\rho u_j'\left(\frac{1}{2}u_i'u_i'\right)}\right]}_{tr_{ff}} \\ & \underbrace{-\bar{u}_i'\frac{\partial\bar{p}}{\partial x_i}}_{pw_f} + \underbrace{\frac{\partial\overline{p'u_i'}}{\partial x_i}}_{pd_f} \underbrace{-\overline{p'\frac{\partial u_i'}{\partial x_i}}}_{pl_f}\end{aligned} \tag{24}$$

where

$$\frac{\mathrm{D}}{\mathrm{D}t} = \frac{\partial}{\partial t} + u_j\frac{\partial}{\partial x_j} \tag{25}$$

and

$$\frac{\overline{\mathrm{D}}}{\mathrm{D}t} = \overline{u_j}\frac{\partial}{\partial x_j} \tag{26}$$

This decomposition allows us to distinguish between the mean flow of stagnation pressure (15) and the flux of stagnation pressure (24) budget. The first one is akin to the commonly used mass-averaged stagnation pressure loss coefficient, which is favored due to the relative ease of measuring it experimentally. The second one corresponds to the correct estimate of loss, but cannot be easily measured experimentally. The difference between the two, which has been highlighted earlier, is due to the presence of turbulent transport terms as well as pressure work, dilation, and diffusion terms. While the last three terms were found to be negligible, the turbulent transport terms, also known as the Reynolds stress work on boundaries, were found to play a significant role for the conditions considered here. These conditions are of relevance to many cascade experiments that feature high levels of unsteadiness at the inflow.

9 Conclusions

A series of high fidelity datasets of compressor cascades at varying inflow conditions was analyzed in this article. For each of the cases, a comparison between entropy, enthalpy, and stagnation pressure loss coefficient was carried out. To understand the difference between the entropy loss coefficient and stagnation pressure loss coefficient, a transport equation budget was performed for both terms. This resulted in the following list of conclusions. While entropy and enthalpy gave almost identical loss predictions, stagnation pressure loss coefficient was found to be unreliable loss metric for cases considered here underpredicting loss for one of the cases by as much as 40% when compared to the entropy loss coefficient (*NACA*65 *Gap*30 case). This was the case despite all the simulations were run at adiabatic and low Mach number conditions. The use of stagnation pressure estimate discarding turbulent kinetic energy resulted in even more unreliable predictions highlighting the importance of including it when comparing experimental data with RANS for highly unsteady flowfields. To understand the discrepancy between loss coefficients, entropy and stagnation pressure transport equation budgets were performed. All the budgets were fully balanced and allowed to elucidate the origin of the discrepancy. This was traced to the turbulent transport terms that arise as part of the stagnation pressure transport equation. These terms were found to be primarily present in the freestream. A

commonly used assumption of its negligible contribution to the overall budget was found to be wrong even when only moderate levels of inflow turbulence were present. The combined impact of these terms was found to be negative for a compressor, resulting in artificially lower loss estimates by the mass-averaged stagnation pressure loss coefficient. This was linked to flow deceleration in a compressor. For a turbine flow, loss estimates are likely to be artificially higher due to the flow acceleration. The use of stagnation pressure loss coefficient may still be valid when low levels of inflow unsteadiness are present and when turbulent transport is low. The impact also appears to be more pronounced for the cases at lower Reynolds number. In addition, it was shown that integrated turbulent transport terms were low within the boundary layers and wake. As a result, loss predicted by entropy and stagnation pressure in those regions was in good agreement. In experimental setting, however, such decomposition may be difficult to achieve, while estimating turbulent transport is beyond current standard experimental practice.

Acknowledgment

The authors would also like to acknowledge the help of UK Turbulence Consortium funded by the EPSRC (Grant No. EP/L000261/1) and Cambridge Service for Data Driven Discovery system operated by the University of Cambridge Research Computing Service funded by EPSRC Tier-2 (Grant No. EP/P020259/1), whose HPC allocations have been used to obtain the results. This project has received funding from the European Union's Horizon 2020 research and innovation programme under the Marie Sklodowska-Curie (Grant No. [101026928]), and this support is also gratefully acknowledged. We also acknowledge PRACE, which awarded access to the Fenix Infrastructure resources at CINECA, partially funded from the European Union's Horizon 2020 research and innovation program through the ICEI project (Grant No. 800858).

Conflict of Interest

There are no conflicts of interest.

Data Availability Statement

The datasets generated and supporting the findings of this article are obtainable from the corresponding author upon reasonable request.

Nomenclature

h = enthalpy
p = pressure
q = heat transfer
s = entropy
u = velocity
x = quantity x
$\dot{m}$ = mass flowrate
$\bar{x}$ = time-average of x
T = temperature
X = volume integral of x
g_{ax} = axial gap
ts_T = entropy generation rate
x_f = related to fluctuating flowfield
x_{ff} = related to the action of fluctuating flowfield on itself
x_i = component of a vector quantity
x_m = related to mean flowfield
x_{mf} = related to the action of both mean and fluctuating flowfields
x_t = related to stagnation quantity
C_{ax} = axial chord
F_{red} = reduced frequency
X_{blw} = quantity integrated over the boundary layer and wake regions
X_{free} = quantity integrated over the freestream region
X_{tot} = quantity integrated over the entire domain
x' = fluctuating component of x
x^h = related to enthalpy
x^p = related to pressure
x^s = related to entropy
$f.sp.$ = flux of stagnation pressure
LHS = left-hand side
Ma = Mach number
Pu = periodic intensity
RANS = Reynolds-averaged Navier–Stokes
Re = Reynolds number based on inlet cond. and axial chord
RHS = right-hand side
Tr = energy transfer between flowfields (turbulence production)
Tu = turbulence intensity
TKE = turbulent kinetic energy

Greek Symbols

Δ_n^+ = viscous wall units in wall-normal dir.
Δ_t^+ = viscous wall units in streamwise dir.
Δ_z^+ = viscous wall units in spanwise dir.
ε = artificial dissipation
ρ = density
τ = shear stress
ϕ = viscous dissipation
Φ = integrated viscous dissipation
ω = loss coefficient
Ω = volume of a domain

Appendix: Double Decomposition of Kinetic Energy

Considerable insight can be drawn from the analysis of kinetic energy budget. Using Reynolds decomposition, kinetic energy can be decomposed into mean (m) and fluctuating (f) components (full derivation available, e.g., in Ref. [27]):

$$\underbrace{\frac{\bar{D}}{Dt}\left(\bar{\rho}\frac{1}{2}\bar{u}_i\bar{u}_i\right)}_{adv_m} = \underbrace{-\bar{u}_i\frac{\partial \bar{p}}{\partial x_i}}_{pw_m} \underbrace{-\left(-\overline{\rho u_i' u_j'}\frac{\partial \bar{u}_i}{\partial x_j}\right)}_{t_{mf}} \underbrace{-\frac{\partial}{\partial x_j}\left[\bar{u}_i\left(\overline{\rho u_i' u_j'}\right)\right]}_{tr_{mf}} + \underbrace{\frac{\partial \bar{\tau}_{ij}\bar{u}_i}{\partial x_j}}_{vd_m} \underbrace{-\bar{\tau}_{ij}\frac{\partial \bar{u}_i}{\partial x_j}}_{\phi_m} \tag{A1a}$$

$$\underbrace{\frac{\bar{D}}{Dt}\left(\bar{\rho}\frac{1}{2}\overline{u_i' u_i'}\right)}_{adv_f} = \underbrace{\left(-\overline{\rho u_i' u_j'}\frac{\partial \bar{u}_i}{\partial x_j}\right)}_{t_{mf}} \underbrace{-\frac{\partial}{\partial x_j}\left[\overline{\rho u_j'\left(\frac{1}{2}u_i' u_i'\right)}\right]}_{\mathrm{tr}_{ff}} + \underbrace{\frac{\partial \overline{\tau_{ij}' u_i'}}{\partial x_j}}_{vd_f} \underbrace{-\overline{\tau_{ij}'\frac{\partial u_i'}{\partial x_j}}}_{\phi_f} \underbrace{-\bar{u}_i'\frac{\partial \bar{p}}{\partial x_i}}_{pw_f} \underbrace{-\frac{\partial \overline{p' u_i'}}{\partial x_i}}_{pd_f} + \underbrace{\overline{p'\frac{\partial u_i'}{\partial x_i}}}_{pl_f} \tag{A1b}$$

where

$$\frac{\bar{\mathrm{D}}}{\mathrm{D}t} \equiv \frac{\partial}{\partial t} + \bar{u}_j\frac{\partial}{\partial x_j} \tag{A2}$$

and

adv: convection of kinetic energy, pw: pressure work, t: energy transfer between mean and fluctuating flowfield (turbulence production), tr: diffusion due to unsteadiness/turbulence, vd: viscous

Table 8 Double decomposition—mean kinetic energy budget

$$\mathrm{Adv}_m = -\mathrm{PW}_m + \mathcal{T}_{mf} - \mathrm{Tr}_{mf} + \mathrm{VD}_m - \Phi_m$$

	NACA65		*NACA65*			*CDA*		
	Tu4	Tu6	Gap30	Gap40	Gap50	Gap30	Gap40	Gap50
Adv_m	111.1445	110.9216	107.7270	109.5839	109.9521	46763.7137	46822.3687	46945.5559
PW_m	−105.2509	−106.1870	−105.9626	−106.2991	−105.8217	−45480.7915	−45432.2649	−45490.2992
$\mathcal{T}_{mf}$	3.1712	3.3751	2.3372	2.4060	2.5776	695.0648	750.2811	780.8226
Tr_{mf}	0.8466	2.5871	3.9051	2.5509	2.0044	387.6402	207.1210	208.5881
VD_m	0.0118	0.0090	0.0139	0.0145	0.0147	2.4507	2.2288	2.2402
Φ_m	3.5879	3.6597	3.4189	3.4715	3.5539	962.0147	904.6694	911.7720
LHS–RHS	−0.0070	0.2958	−0.0727	−0.0273	0.0179	15.9336	−55.4968	−26.5095

Table 9 Double decomposition—turbulent kinetic energy budget

$$\mathrm{Adv}_f = -\mathrm{PW}_f + \mathcal{T}_{mf} - \mathrm{Tr}_{ff} + \mathrm{VD}_f - \Phi_f - \mathrm{PD}_f + \mathrm{PL}_f$$

	NACA65		*NACA65*			*CDA*		
	Tu4	Tu6	Gap30	Gap40	Gap50	Gap30	Gap40	Gap50
Adv_f	0.7976	2.8418	2.0468	1.5165	1.1772	533.4470	501.4282	474.7137
PW_f	—	—	—	—	—	—	—	—
$\mathcal{T}_{mf}$	3.1712	3.3751	2.3372	2.4060	2.5776	695.0648	750.2811	780.8226
Tr_{ff}	0.0000	0.0000	−0.6882	−0.6488	−0.4883	−94.2817	−213.8627	−202.5755
VD_f	0.0083	0.0167	0.0052	0.0050	0.0051	1.8809	1.5766	1.5437
Φ_{f+N}	3.9764	6.2947	3.5608	3.1964	3.1722	1149.2538	1011.4609	1004.9839
PD_f	—	—	−0.1294	−0.0801	−0.1112	−4.8095	−26.3358	−33.4561
PL_f	—	—	—	—	—	—	—	—
LHS–RHS	0.0007	-0.0610	0.0108	0.0021	-0.0118	-17.9523	1.6265	16.0645

diffusion, ϕ: viscous dissipation, pd: pressure diffusion, pl: pressure dilation.

Table 8 shows that mean kinetic energy budgets is satisfied. For turbulent kinetic energy budget, the balance was achieved when artificial dissipation was added to the resolved dissipation, Table 9. This further validates the methodology taken in this study.

References

[1] Sandberg, R. D., and Michelassi, V., 2022, "Fluid Dynamics of Axial Turbomachinery: Blade-and Stage-Level Simulations and Models," Annu. Rev. Fluid. Mech., **54**, pp. 255–285.
[2] Denton, J. D., 1993, "Loss Mechanisms in Turbomachines," ASME J. Turbomach., **115**(4), pp. 621–656.
[3] Miller, R. J., 2013, "Mechanical Work Potential," Turbo Expo: Power for Land, Sea, and Air, ASME Paper No. GT2013-95488, American Society of Mechanical Engineers.
[4] Moore, J., Shaffer, D., and Moore, J., 1987, "Reynolds Stresses and Dissipation Mechanisms Downstream of a Turbine Cascade," ASME J. Turbomach., **109**(2), pp. 258–267.
[5] Tennekes, H., and Lumley, J., 1972, *A First Course in Turbulence*, MIT Press, Cambridge, MA.
[6] Stieger, R. D., and Hodson, H. P., 2005, "The Unsteady Development of a Turbulent Wake Through a Downstream Low-Pressure Turbine Blade Passage," ASME J. Turbomach., **127**(2), pp. 388–394.
[7] MacIsaac, G., Sjolander, S., and Praisner, T., 2012, "Measurements of Losses and Reynolds Stresses in the Secondary Flow Downstream of a Low-Speed Linear Turbine Cascade," ASME J. Turbomach., **134**(6), p. 061015.
[8] Lengani, D., Simoni, D., Ubaldi, M., Zunino, P., Bertini, F., and Michelassi, V., 2017, "Accurate Estimation of Profile Losses and Analysis of Loss Generation Mechanisms in a Turbine Cascade," ASME J. Turbomach., **139**(12), p. 121007.
[9] Wu, X., and Durbin, P. A., 2001, "Evidence of Longitudinal Vortices Evolved From Distorted Wakes in a Turbine Passage," J. Fluid Mech., **446**, pp. 199–228.
[10] Michelassi, V., and Wissink, J. G., 2015, "Turbulent Kinetic Energy Production in the Vane of a Low-Pressure Linear Cascade With Incoming Wakes," Int. J. Rot. Mach., **2015**, p. 650783.
[11] Wheeler, A. P., Sandberg, R. D., Sandham, N. D., Pichler, R., Michelassi, V., and Laskowski, G., 2016, "Direct Numerical Simulations of a High-Pressure Turbine Vane," ASME J. Turbomach., **138**(7), p. 071003.
[12] Przytarski, P. J., and Wheeler, A. P., 2020, "The Effect of Gapping on Compressor Performance," ASME J. Turbomach., **142**(12), p. 121006.
[13] Leggett, J., Richardson, E., Priebe, S., Shabbir, A., Michelassi, V., and Sandberg, R., 2020, "Loss Analysis of Unsteady Turbomachinery Flows Based on the Mechanical Work Potential," ASME J. Turbomach., **142**(11), p. 111009.
[14] Przytarski, P. J., and Wheeler, A. P., 2021, "Accurate Prediction of Loss Using High Fidelity Methods," ASME J. Turbomach., **143**(3), p. 031008.
[15] Leggett, J., Zhao, Y., Richardson, E. S., and Sandberg, R. D., 2021, "Turbomachinery Loss Analysis: The Relationship Between Mechanical Work Potential and Entropy Analyses," Turbo Expo: Power for Land, Sea, and Air, ASME Paper No. GT2021-59436, American Society of Mechanical Engineers.
[16] Miki, K., and Ameri, A., 2024, "Numerical Investigation of the Effect of Trailing Edge Thickness of Simulated CMC Blades on Loss Profiles," ASME J. Turbomach., **146**(9), p. 091009.
[17] Wheeler, A. P. S., Dickens, A. M. J., and Miller, R. J., 2018, "The Effect of Non-equilibrium Boundary Layers on Compressor Performance," ASME J. Turbomach., **140**(10), p. 101003.
[18] Brown, L. E., 1972, "Axial Flow Compressor and Turbine Loss Coefficients: A Comparison of Several Parameters," ASME Conference Proceedings, ASME Paper No. 72-GT-18.
[19] Jardine, L., 2019, *The Effect of Heat Transfer on Turbine Performance*, University of Cambridge, Cambridge, UK.
[20] Cantwell, B., 2013, *AA200: Applied Aerodynamics*, Stanford University, Stanford, CA.
[21] Zhao, Y., and Sandberg, R. D., 2020, "Using a New Entropy Loss Analysis to Assess the Accuracy of RANS Predictions of an High-Pressure Turbine Vane," ASME J. Turbomach., **142**(8), p. 081008.
[22] Hinze, J. O., 1975, *Turbulence*, McGraw Hill, New York.
[23] Perdichizzi, A., Ubaldi, M., and Zunino, P., 1990, "A Hot Wire Measuring Technique for Mean Velocity and Reynolds Stress Components in Compressible Flow," Measuring Techniques in Turbomachinery, Paper No. MTT1090, American Society of Mechanical Engineers.
[24] Jelly, T. O., Day, I. J., and di Mare, L., 2017, "Phase-averaged Flow Statistics in Compressors Using a Rotated Hot-Wire Technique," Exp. Fluids, **58**(48), pp. 1–7.
[25] Folk, M., 2019, *The Impact of Combustor Turbulence on Loss Mechanisms in the High Pressure Turbine*, University of Cambridge, Cambridge, UK.
[26] Folk, M., Miller, R. J., and Coull, J. D., 2020, "The Impact of Combustor Turbulence on Turbine Loss Mechanisms," ASME J. Turbomach., **142**(9), p. 091009.
[27] Aupoix, B., Blaisdell, G. A., Reynolds, C. W., and Zeman, O., 1990, "Modelling the Turbulent Kinetic Energy Equations for Compressible, Homogeneous Turbulence," Proceedings of the Summer Program 1990, Center for Turbulence Research, Paper No. N92-30653.